Controllable Synthesis of Mesoporous TiO_2 Hollow Shells: Toward an Efficient Photocatalyst

*Ji Bong Joo, Ilkeun Lee, Michael Dahl, Geon Dae Moon, Francisco Zaera, and Yadong Yin**

TiO_2 hollow shells with well-controlled crystallinity, phase, and porosity are desirable in many applications. In photocatalysis in particular, they can provide high active surface area, reduced diffusion resistance, and improved accessibility to reactants. Here, the results from studies of the causes for the failure of a prior etching and calcination scheme to make such shells and on a newly-developed simple yet robust process for producing uniform mesoporous TiO_2 shells with precisely controllable crystallinity and phase are reported. The key finding is that base etching of the SiO_2@TiO_2 core-shell particles leads to the formation of sodium titanate species, which, if not removed, promote substantial crystal growth during calcination and destroy the structural integrity of the TiO_2 shells. A simple acid treatment of the base-etched samples may convert the sodium titanates into protonated titanates, which not only prevent the formation of the impurity phases, but also help to maintain the structural integrity of the shell and allow precise control of the TiO_2 phase and crystallinity. This new development affords convenient optimization of the structure of the hollow TiO_2 shells toward efficient photocatalysts, which outperform the commercial P25-TiO_2 in the photocatalytic decomposition of organic dye molecules.

1. Introduction

Titanium dioxide (titania, TiO_2) has proven a quite versatile material, being useful in various practical applications such as bio-separation, energy storage, solar cells, catalysis, and photocatalysis.[1] Under UV light irradiation, with photons of energy above the wide band-gap (3.0–3.2 eV) of TiO_2, light absorption leads to the generation of electron (e^-)-hole (h^+) pairs which can induce a variety of redox reactions. Since the first demonstration of the electrochemical photolysis of water, TiO_2 has been intensively studied and used as photocatalyst in both fundamental research and practical applications.[2] Over the past few decades, tremendous effort has been devoted to improving the catalytic activity of TiO_2-based photocatalysts.[3]

It is generally agreed that the performance of TiO_2 photocatalysts may be improved by developing materials with well-controlled characteristics such as high crystallinity, large surface area, and high porosity.[3b] With the continuous developments in the synthetic chemistry of nanomaterials, new classes of nanostructured TiO_2 materials have been prepared and investigated for photocatalysis.[4] In principle, well-dispersed anatase TiO_2 colloidal nanocrystals should be the ideal form of photocatalyst, since those can maximize the catalytically active surface area.[5] However, in order to maintain colloidal stability, nanocrystals synthesized by conventional solution-phase methods are typically covered with organic capping ligands, and those significantly hamper photocatalytic activity by limiting the access of the reactants to the nanocrystal surface.[6] To address this issue, TiO_2 photocatalysts are often produced in the form of a mesoporous framework that can be calcined at high temperatures to ensure a clean surface, a high surface area, and well developed crystallinity.[4a,7] It has been further suggested that preparation of mesoporous TiO_2 in colloidal form with sub-micrometer dimensions can facilitate mass transfer during catalytic reactions. An additional benefit of making catalysts in microsphere form is that they can usually be stabilized by the electrostatic charges carried on their surfaces, so that no additional capping ligands are needed for maintaining dispersion stability. The relatively larger size of microspheres compared to typical nanoparticles also makes them easier to recycle from the reaction media, by, for example, centrifugation.[8] If the core region of a colloidal particle is denser than the surface, additional improvements in performance may be achieved by removing the core portion to produce a porous hollow shell; such shells are expected to display more active sites per unit mass, reduced diffusion resistance, and improved accessibility of the reactant to the active surface.[9]

Several synthetic methods have been reported to create TiO_2 hollow shells, typically through ripening or templating processes.[10] Hydrothermal treatments are often used for preparing crystalline TiO_2 hollow shells, either with or without the use of additional sacrificial templates.[1d,10c,11] However, as with many other hydrothermal reactions, these processes are simple and convenient but are usually carried out under high pressures in sealed reactors, and under such conditions it is difficult to monitor the growth and precisely control the shell thickness, porosity, and crystallinity of the products.

We have previously reported a robust sol-gel coating procedure for producing amorphous TiO_2 shells on templates such

Dr. J. B. Joo, Dr. I. Lee, M. Dahl, Dr. G. D. Moon,
Prof. F. Zaera, Prof. Y. Yin
Department of Chemistry
University of California
Riverside, CA, 92521, USA
E-mail: yadong.yin@ucr.edu

DOI: 10.1002/adfm.201300255

as SiO_2 colloids.[12] In principle, crystalline hollow TiO_2 shells can be produced by further calcination of the SiO_2@TiO_2 core-shell particles at high temperatures followed by selective etching of the SiO_2 core with a strong base such as NaOH. In practice, however, a simple calcination process cannot maintain the shell morphology due to the significant structural rearrangement in the TiO_2 shells associated with the extensive crystallization and grain growth during calcination. In a reverse process, amorphous TiO_2 shells are first produced by etching the sol-gel derived SiO_2@TiO_2 core-shell particles and then calcined at high temperature. This, however, leads to the formation of a significant amount of sodium titanate impurities, and also to largely damaged shell morphology.[9b] To produce mesoporous crystalline shells, we have also developed a silica protected calcination process, which relies on an additional silica coating to limit the structural rearrangement of titania during calcination. Although a well-developed mesoporous shell with a high surface area (>300 m^2/g) can be obtained this way, control of the anatase crystalline grains is limited to sizes of approximately 5 nm in diameter even at considerably high calcination temperatures, around 900 °C. This is because of the significant inhibition that the impregnated silicate species exert on the TiO_2 crystallization. A partial etching and re-calcination strategy was then proposed to enhance the crystallinity of the anatase grains of TiO_2 shells while at same time maintaining the shell morphology.[9a] Since the impregnated silicate species in the TiO_2 matrix have a more disrupted Si-O-Si network compared to other silica-rich regions, they can be preferentially etched away to allow further controlled growth of anatase crystalline grains through a re-calcination process. This does result in hollow TiO_2 shells with a well-developed anatase crystallinity, considerable surface area, and subsequently enhanced photocatalytic activity. The drawback of this strategy, however, is that the procedure is quite complicated, involving multiple steps of coating, etching, and calcination. A simpler process that allows maintaining the mesoporous shell morphology and controlling the crystallinity would be highly desirable.

In this paper, we report on our studies of the causes for the failure of the prior etching and calcination scheme, and describe a new simpler yet robust process for producing uniform mesoporous TiO_2 shells with highly controllable crystallinity and phases. The key finding of this work is that the base etching of amorphous titania leads to the formation of sodium titanate species which, if not removed, crystallize substantially during calcination and destroy the structural integrity of the TiO_2 shells. We found that a simple acid treatment of the base-etched samples may convert the sodium titanates into protonated titanates, which not only prevent the formation of the impurity phases but also help maintain the hollow morphology of the shells and allow precise control of the development of the TiO_2 crystalline domains. The resulting TiO_2 nanostructures show advantageous characteristics such as uniform particle size, good water dispersity, mesoscale porosity, tunable crystallinity, and controllable crystalline phase. The new process reported here affords the convenient optimization of the structure of the hollow TiO_2 shells to achieve higher photocatalytic performance than commercial P25-TiO_2 for the decomposition of organic molecules.

2. Results and Discussion

Amorphous hollow TiO_2 nanostructures can be synthesized by a conventional templating method which combines sol-gel coating and selective etching processes.[12] More specifically, the synthesis involves the preparation of uniform SiO_2 particles, coating with a TiO_2 layer via a sol-gel reaction of tetrabutyl titanate (TBOT) to form SiO_2@TiO_2 core-shell nanostructures, and chemical etching of the SiO_2 core by NaOH to produce hollow TiO_2 shells. Upon direct calcination of the as-synthesized hollow TiO_2 shells at high temperatures, e.g., 800 °C, not only the hollow morphology is completely destroyed (**Figure 1**a), but also an undesired sodium titanate

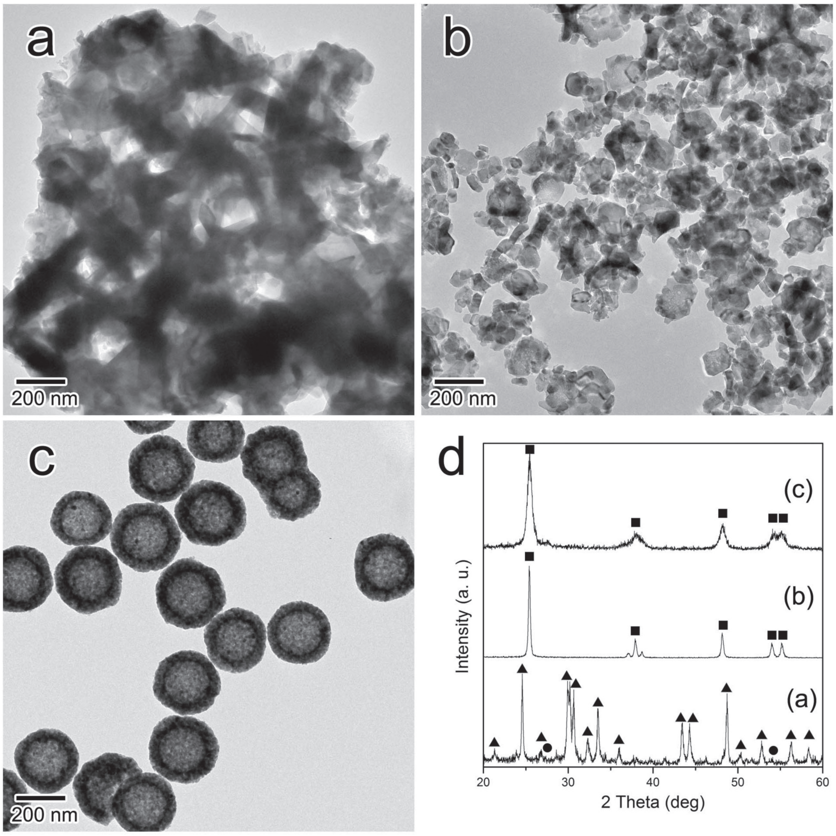

Figure 1. a–c) TEM images of hollow shells prepared following various etching and calcination sequences: a) base etching of silica followed by calcination at 800 °C; b) calcination at 800 °C followed by base etching of silica; and c) base etching of silica followed by acid treatment and then calcination at 800 °C. d) XRD patterns of the corresponding samples (■, ● and ▲ denote anatase, rutile and sodium titanate phases, respectively).

phase is obtained (Figure 1d). The formation of sodium titanate is an interesting result of the templating and base etching processes, but sodium titanate is not a desirable photocatalyst, as its activity is considerably lower than that of anatase TiO_2. We found that the etching of pure sol-gel derived TiO_2 particles by NaOH is rather slow, and that it is difficult to directly convert amorphous TiO_2 into sodium titanate. Apparently, the titania species deposited onto the amorphous silica are key to the formation of the sodium titanate phase upon base etching. As condensation of the amorphous silica synthesized by the sol-gel process is generally far from completion,[13] the large amount of silanol groups contained in both the porous network and the surface react with the titania precursor during the deposition of the titania to form Si-O-Ti bonds. Presumably, the Si-O-Ti bonds break and convert into sodium titanate species ($Ti\text{-}O^-Na^+$) upon selective etching of the silica by NaOH. It is also believed that the presence of sodium titanate causes the destruction of the shell morphology because, as evidenced by the XRD data in Figure 1d, it crystallizes substantially during calcination and produces crystal grains with sizes beyond the thickness of the shells. Even in the case when the original amorphous shells are etched to a lesser extent so that the final products contain a mixture of titania and sodium titanate, it was found that, still, it is difficult to maintain the hollow shell morphology because the fast grain growth of sodium titanate weakens the overall mechanical strength of the shells.[9b] When the reverse process was attempted, i.e., the calcination of the $SiO_2@TiO_2$ core-shell samples before chemical etching of the SiO_2, the final product exhibited a well-crystallized anatase structure (XRD analysis, Figure 1d), but the hollow morphology could not be maintained (TEM image, Figure 1b). In this case, the challenge is to precisely control the crystallization of the TiO_2 layer and grain growth during calcination while avoiding significant structural rearrangement that often leads to the breakage of the shells.

Sodium titanate is known to be a good cation exchanger.[14] We therefore suggested that it should be possible to readily replace the sodium cations by protons to form protonated titanate species which can then be transformed to anatase crystalline TiO_2 by dehydration and crystallization during the calcination.[15] Indeed, a simple treatment of the etched sample with diluted HCl solution was found to be able to convert the detrimental sodium titanate into protonated titanate, helping not only to preserve the pure titania phase but also to maintain the structural integrity of the shell and to allow precise control of the TiO_2 crystallinity. As shown in the representative TEM image in Figure 1c, TiO_2 particles prepared in this way well maintain hollow morphologies as well as high crystallinity, with the major crystalline phase being anatase (Figure 1d).

The acid treatment strategy is not restricted to HCl. Other inorganic acids, including aqueous HNO_3 and H_2SO_4, can also be used for this application. **Figure 2** shows the XRD patterns and representative TEM images of hollow anatase shells prepared by treating the base-etched samples with 1 mmol HNO_3 and 0.5 mmol H_2SO_4 followed by calcinations at 800 °C. Both of the TiO_2 samples showed well-developed anatase crystalline phases in XRD analysis as well as a hollow morphology in the TEM images.

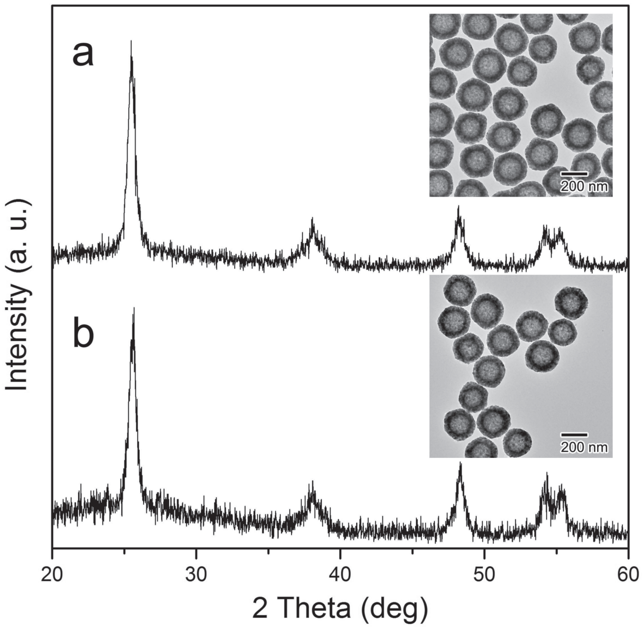

Figure 2. XRD patterns and representative TEM images of hollow anatase TiO_2 nanostructures prepared by treating the etched samples with other inorganic acids followed by calcination at 800 °C: a) 1 mmol HNO_3 and b) 0.5 mmol H_2SO_4.

Additional sample characterization was carried out by using X-ray photoelectron spectroscopy (XPS) to monitor the relative amount of Na^+ cations remaining in amorphous hollow TiO_2 samples after treating with different amounts of HCl. **Figure 3**a shows Na 1s XPS spectra obtained for the amorphous hollow TiO_2 samples after acid treatment. It is clear that a significant amount of Na^+ ions remained in the etched sample even after repeated washing with water, as suggested by the strong Na 1s peak in the XPS pattern for the 0 mmol case (top trace). Upon acid treatment, however, it is clear that the Na^+ ions are easily replaced by H^+ to produce protonated titanate species.[15b,16] Moreover, more extensive Na^+ replacement is obtained with more addition of HCl. By considering atomic sensitivity factors, the relative atomic ratio of Na to Ti for hollow TiO_2 samples treated with solutions of different acid concentrations were calculated and plotted in Figure 3b. The as-etched sample shows a Na/Ti atomic ratio of 1.05, a value that drops to 0.69, 0.49, and eventually 0, as 0.01, 0.1 to 1 mmol of HCl was added to a 150-mg dried solid sample, respectively. The XPS data, together with the XRD measurements described below, clearly supports that the Na^+ cations are removed by ion exchange during acid treatment and that, eventually, no Na^+ is left in the shell matrix. Importantly, the cation exchange process does not lead to major structural reconstruction: the hollow shells maintain their morphology and mesoporous structure, as evidenced by the TEM images in the insets of Figure 3b.

Next, the changes of crystalline phase and crystallinity of acid-treated hollow samples calcined at different temperatures was investigated by XRD. As shown in **Figure 4**a, when calcined at 500 °C, hollow samples treated with 0.01 and 0.1 mmol HCl showed broad diffraction patterns without any apparent peaks, indicating the amorphous nature of the solid. However, the hollow shells treated with 1 mmol HCl showed well-developed

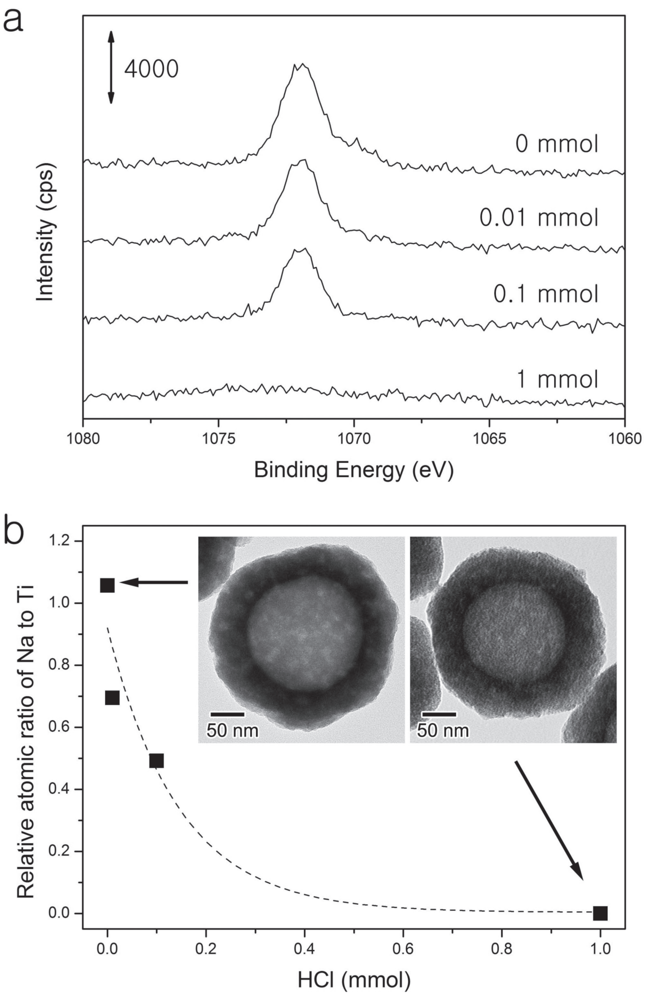

Figure 3. a) Na 1s XPS spectra and b) relative Na/Ti atomic ratios in amorphous hollow TiO_2 samples before and after treatment with HCl solutions of different concentrations. The insets in (b) are representative TEM images of amorphous hollow TiO_2 shells before and after acid treatment.

anatase peaks under the same calcination condition. Moreover, upon calcination at 650 °C, the sample treated with 0.01 mmol HCl yielded an XRD pattern with broad peaks due to a sodium titanate crystalline phase ($Na_2Ti_6O_{13}$, JC-PDS 73-1398#), whereas those treated with 0.1 and 1 mmol HCl were seen to crystallize to the titania anatase phase (Figure 4b). When an even higher calcination temperature was used, e.g. 800 °C, the 0.01 mmol HCl treated sample showed sharp peaks mainly due to sodium titanate phase but also minor signals from rutile TiO_2, whereas the 0.1 mmol HCl treated one displayed mainly peaks for the rutile phase, with minor sodium titanate peaks (Figure 4c). The sample treated with a 1 mmol HCl solution consistently displayed a dominant anatase phase at all calcination temperatures, even at 800 °C, but sharper diffraction peaks were seen with increasing calcination temperature, suggesting enhanced crystallinity.

These results can be explained by noting that the amorphous titania in the shells made in this study are only partially

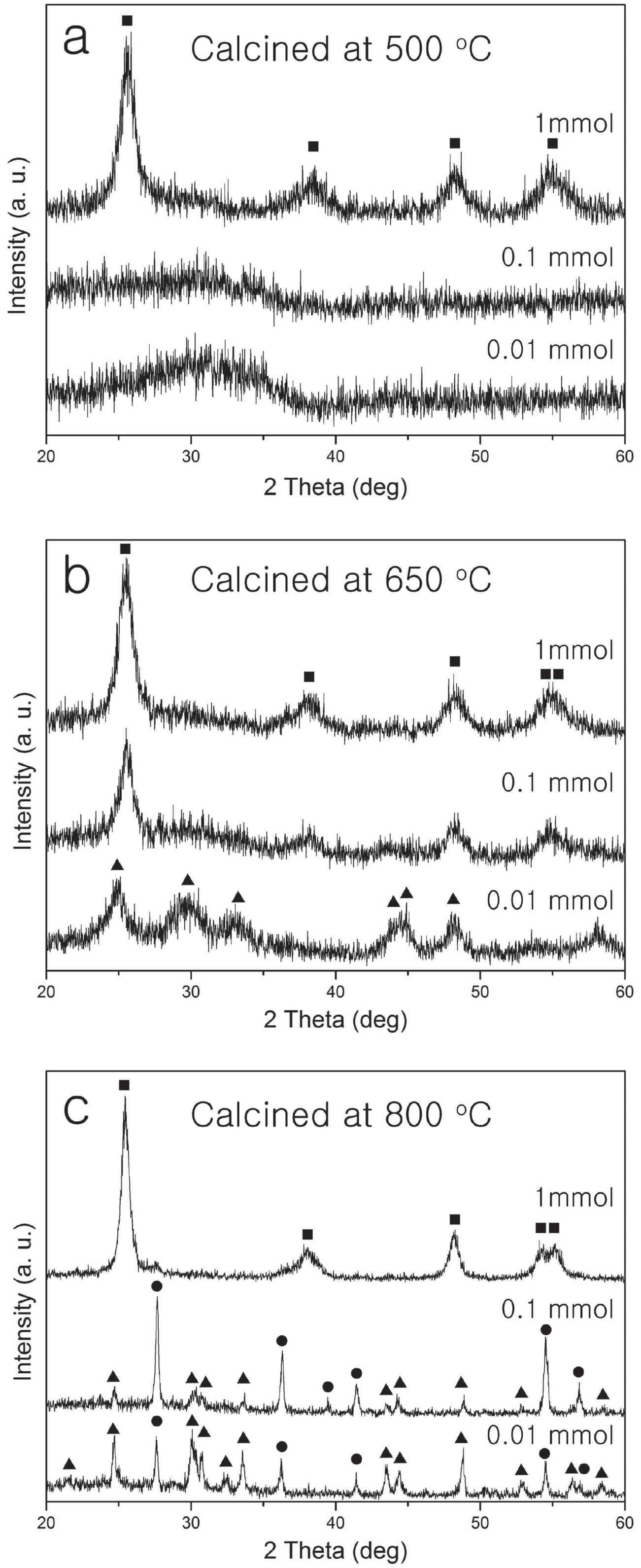

Figure 4. XRD patterns of acid-treated hollow samples calcined at different temperatures: a) 500 °C, b) 650 °C and c) 800 °C. ■, ● and ▲ denote anatase, rutile and sodium titanate phases, respectively.

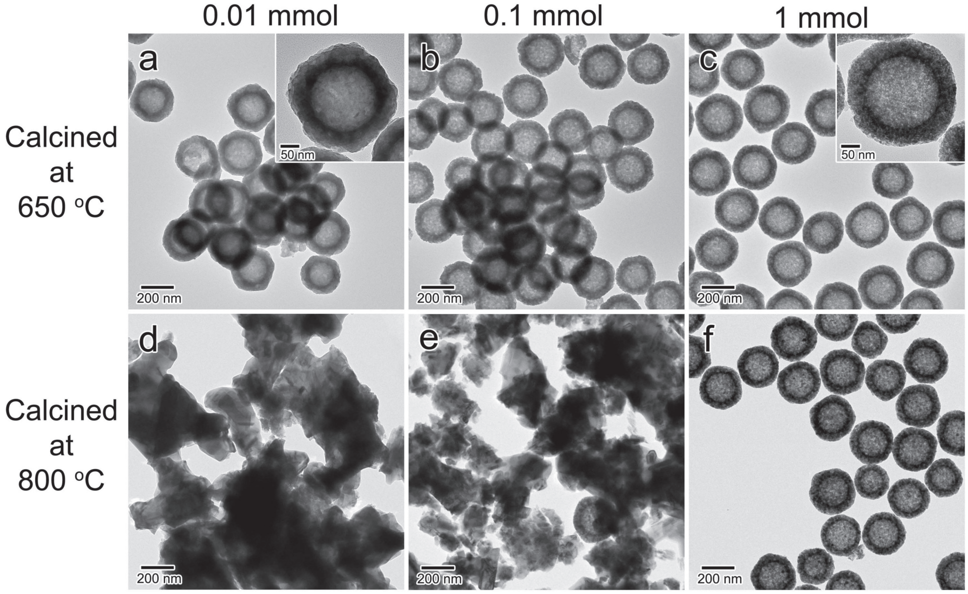

Figure 5. TEM images of TiO_2 samples produced by acid treatment with HCl solutions of different concentrations followed by calcination at a–c) 650 °C or d–f) 800 °C.

converted to sodium titanate during the NaOH etching. When the as-etched hollow samples were treated with dilute HCl, the Na^+ cations were replaced by H^+ ions and the resultant protonated titanate could be dehydrated and then crystallized to different phases depending on how much Na^+ ions remained. In the case of 0.01 mmol HCl treatment, since the extent of the H^+ ion exchange is limited, perhaps amounting to only ≈30% of the total Na^+ content (according to the XPS data, Figure 3), there is still a large number of Na^+ ions in the shell, and that makes it difficult to get a crystalline phase unless high temperatures are used. Moreover, high calcination temperatures in this case lead to the crystallization of sodium titanate, not titania, phases. Only at calcination temperatures of or above 800 °C a small portion of protonated titanate could form a titania crystalline phase, albeit in the form of rutile.

In the intermediate case of the sample treated by 0.1 mmol HCl, a smaller number of Na^+ ions, approximately half of those in the original etched sample, are left in the shell. As a result, it shows a different crystallization behavior during calcination. No extensive crystallization takes place at 500 °C, as in the 0.01 mmol HCl case, but a metastable anatase phase is observed upon calcination at 650 °C, presumably from crystallization of the protonated titanate fraction of the solid sample. At higher calcination temperatures, e.g., 800 °C, the metastable anatase phase transforms to the rutile phase, and a small amount of crystalline sodium titanate forms as well. It is well known that metal cations of small radii and low valence can accelerate the transformation of anatase to rutile owing to the increase in oxygen vacancy resulting from the substitution of Ti^{4+} ions with lower-valence metal cations.[17] During the calcination of the sample treated with the 0.1 mmol HCl solution at 800 °C (and also with the 0.01 mmol HCl), the remaining Na^+ ions in the solid not only contribute to the formation of a minority sodium titanate phase, but also promote the early phase transformation of the shell from anatase to rutile.

The effect of Na^+ cations in promoting the anatase-to-rutile phase transformation is also evidenced by the fact that the sample treated with 1 mmol HCl, which had no remaining Na^+ ions, still exhibited a major well-developed anatase phase after calcination at 800 °C. This anatase phase forms from crystallization of the amorphous protonated titanate phase.[15] It is believed that this protonated titanate plays a role similar to amorphous silica in limiting the grain growth of titania and delaying the phase transformation from anatase to rutile.[9b] As a result, it is possible to control the grain size of the shell within a considerably wide range of diameters while at the same time retaining the anatase phase, which is preferred for photocatalysis. As discussed later, the existence of protonated titanate is also beneficial for the formation of mesoscale porosity and for maintaining a relatively high surface area. Upon further increases of the calcination temperature, to over 900 °C, phase transformations can still occur, and the rutile phase can appear (see below).

The variation in the concentration of the acid used in the ion exchange treatment not only affects the crystal structure but also the morphology of the shells made after calcination at high temperatures. This is shown in the TEM images in **Figure 5**. When acid-treated samples were calcined at relatively low temperatures, e.g., 650 °C, all samples retained a shell morphology (Figure 5a–c). However, the sample treated with 1 mmol HCl developed a highly porous structure consisting of small crystalline grains, as indicated by the high magnification images in the insets of Figure 5a,c. As the calcination temperature was increased to 800 °C, the samples treated with 0.01 and 0.1 mmol HCl showed completely broken morphology, whereas the one treated with 1 mmol HCl still maintained a uniform hollow shell morphology. Based on the XRD and TEM studies discussed above, we can conclude that the amount of sodium left in the TiO_2 layer after acid treatment is essential in determining not only the crystalline phase but also microscopic

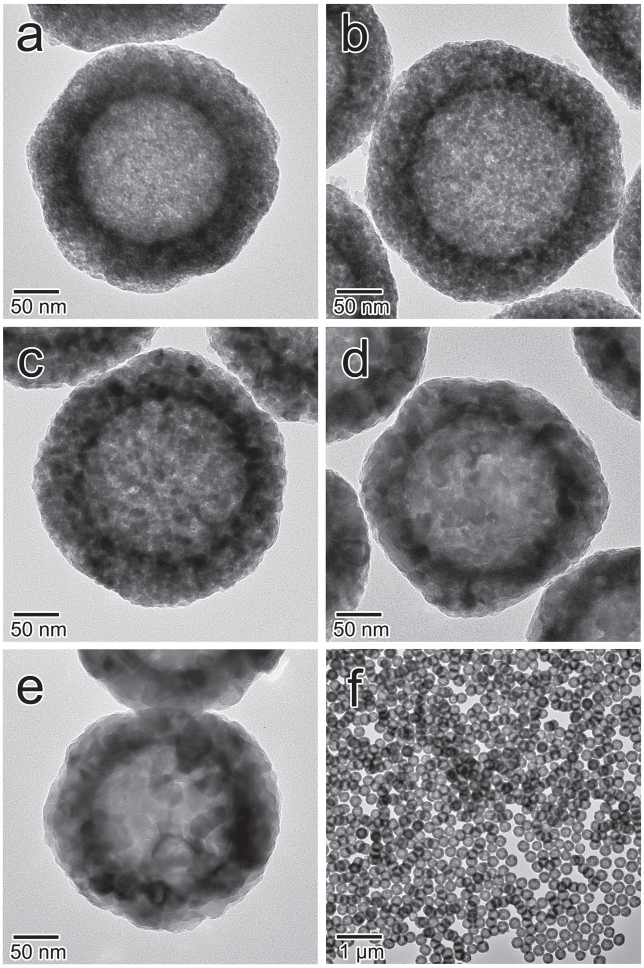

Figure 6. TEM images of hollow TiO_2 shell structures prepared by acid treatment with 1 mmol HCl and then calcination at different temperatures: a) 500 °C (H-TiO_2-500), b) 650 °C (H-TiO_2-650), c) 800 °C (H-TiO_2-800), d) 900 °C (H-TiO_2-900) and e,f) 950 °C (H-TiO_2-950).

morphology of the final products. Since treatment with 1 mmol HCl leads to the formation of a pure anatase TiO_2 phase as well as to the retention of the hollow shell structure, we will focus our subsequent discussion on the samples prepared that way. The samples will be denoted as H-TiO_2-x, with x being the calcination temperature.

Figure 6 compares the development of the crystalline grains of the final hollow TiO_2 shells after being calcined at different temperatures. The sample calcined at 500 °C has the smallest crystal grains (≈6 nm, Figure 6a), and the average crystal grain size increases continuously with increasing calcination temperature (Figure 6b–e). Based on a closer observation of the TEM images, one can also see that the porosity of the TiO_2 shell layer is significantly reduced in the samples calcined at higher temperatures. It should be noted that the hollow shell structure can be well maintained even after the samples are calcined at high temperatures (i.e., 950 °C), as shown in the low magnification TEM image in Figure 6f.

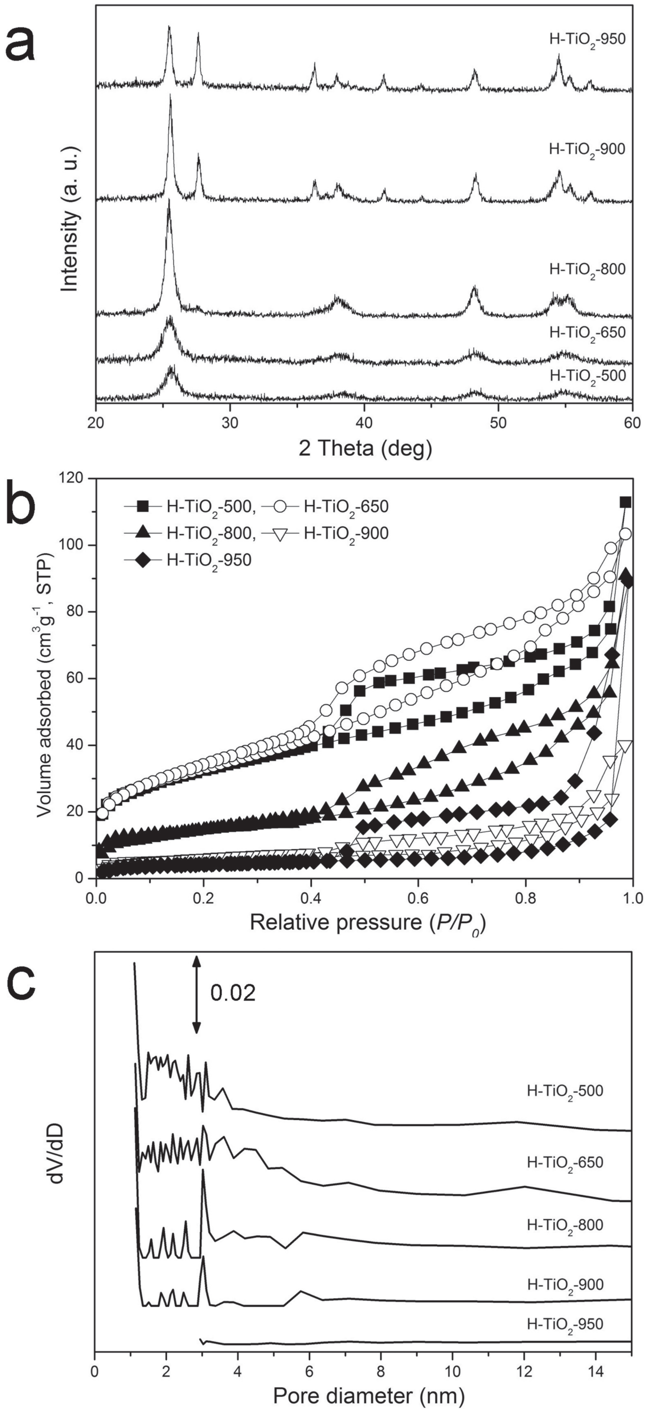

Figure 7. a) XRD patterns, b) N_2 adsorption isotherms, and c) BJH pore size distribution obtained for hollow TiO_2 shells prepared by acid treatment with 1 mmol HCl and then calcination at different temperatures.

The crystal grain growth, crystalline phase changes, and porosity of the hollow TiO_2 samples treated with 1 mmol HCl and calcined at different temperatures were investigated by XRD and N_2-adsorption techniques. As shown in **Figure 7**a, the hollow TiO_2 sample calcined at 500 °C (H-TiO_2-500) displayed relatively broad peaks for the anatase phase at $2\theta = 25.4$, 37.9, 48.1, 54 and 55°, which are attributed to the (101), (004), (200), (105) and (211) planes respectively. As the calcination temperature was increased, the relative intensity and sharpness of the peaks increases, indicating enhanced crystallinity, and by 900 °C and 950 °C new XRD peaks were seen at $2\theta = 27.6$, 36.6, 38.0, 41.4 and 54.5° corresponding to the rutile phase (the (110), (101), (111), (210) and (211) planes, respectively), together with a reduction in the peak intensity ratios of the anatase to rutile phases. The average anatase grain sizes of the TiO_2 samples, calculated from the widths of the anatase (101) peak in the XRD data by using the Scherrer formula,[18] were estimated at approximately 6.9, 7.1, 12.1, 19 and 20 nm for sample heated at 500 °C, 650 °C, 800 °C, 900 °C, 950 °C, respectively, and the rutile grain size of samples calcined at 900 °C and 950 °C were estimated (by using the rutile (110) peak) at 25.2 and 27.5 nm, respectively. These results are consistent with the TEM observations in Figure 6.

Figure 7b,c show the N_2 adsorption-desorption isotherms and the corresponding Barrett-Joyner-Halenda (BJH) pore size distributions obtained for the same TiO_2 shell samples. All samples displayed type IV isotherms with a hysteresis loop indicating mesoporous characteristics. The hollow TiO_2 samples calcined at relatively low temperatures, e.g., 500 °C and 650 °C, showed large adsorption volumes in the monolayer region, indicating porous structures with high BET surface areas, but those monolayer adsorption volumes decreased monotonically with increasing annealing temperature, indicating decreasing porosity and surface area, again consistent with the trends observed in the TEM analysis (Figure 6). The measured surface areas for the hollow TiO_2 samples calcined at 500, 650, 800, 900 and 950 °C were 115, 118, 50, 19 and 14 m^2/g, respectively. Although there are no sharp distribution peaks in the BJH pore size distribution curves, all samples show pores with sizes in the range of 2 to 10 nm (Figure 7c).

The photocatalytic activity of the H-TiO_2-x samples was evaluated by monitoring the degradation of Rhodamine B (RhB) under UV irradiation versus time. **Figure 8** displays the data in semilogarithmic form in order to highlight the first order nature of the reaction and to facilitate the calculation of first-order reaction rate constants (k). Only minor degradation (4.5% in 30 min) was observed in a blank test (without catalyst), corresponding to a reaction rate constant of approximately 0.0009 min^{-1}. The photocatalytic activity of titania is indicated by the results obtained by using a commercial TiO_2-P25 sample, for which a reaction rate constant of 0.17 min^{-1} was measured. Our titania shell catalyst display similar or better activity than the P25 sample. Specifically, the H-TiO_2-500 showed the lowest k value among all catalysts tested in this work (0.033 min^{-1}). However, the k value increased continuously as the calcination temperature was increased all the way to 800 °C ($k = 0.102$ and 0.200 min^{-1} for H-TiO_2-650 and H-TiO_2-800, respectively), then decreased for the sample calcined at 900 °C ($k = 0.117$ min^{-1}). The H-TiO_2-800 shows the highest k value, outperforming the commercial P25-TiO_2 catalyst. In addition, the photocatalytic activity of H-TiO_2-800 was well maintained during 5 cycles of repeated reactions, indicating excellent chemical and optical stability (Figure S1, Supporting Information).

Our hollow TiO_2 catalysts display relative high adsorption capacity, in the range of 11–13% of C/C_0. This is to be compared with a value of 6% for the commercial P25-TiO_2. This difference in adsorption capacity may come from differences in surface properties. Specifically, the zeta potential values of the TiO_2 samples dispersed in deionized water were found to be ca. −38, −53 and +66 mV for the H-TiO_2-500, H-TiO_2-800 and P25-TiO_2, respectively. The negative surface charges of these samples contribute to their higher adsorption capacity than P25-TiO_2 as they tend to attract more positively-charged RhB molecules in aqueous solutions with a neutral pH. The high density of negative charges on the surface of the calcined samples also contributes to their excellent water dispersibility, a beneficial feature for good photocatalytic performance.

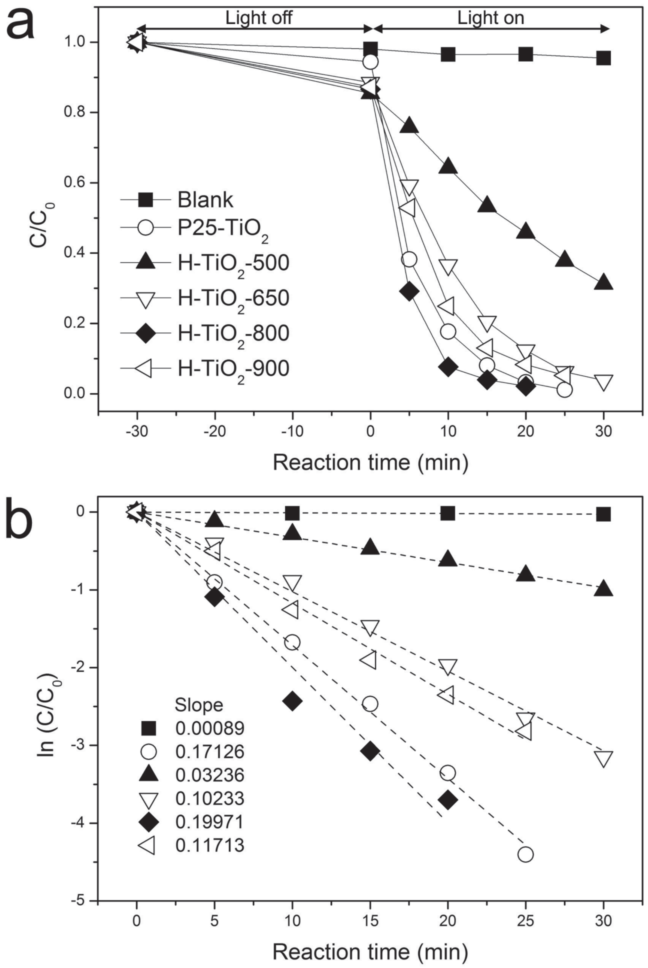

Figure 8. a) Photocatalytic degradation of RhB under UV light irradiation and b) apparent reaction rate constant vs. reaction time in the presence of different TiO_2 catalysts: blank experiment (without catalyst) (■), commercial P25-TiO_2 (○), H-TiO_2-500(▲), H-TiO_2-650 (▽), H-TiO_2-800 (◆), and H-TiO_2-900 (◁)).

As we have pointed out in our previous studies, many factors play a role in defining photocatalytic activity, with improvements seen with high crystallinity, a large surface area, and having the right crystalline phase.[9a] In the system reported here, it is clear that higher calcination temperatures are helpful in improving the anatase crystallinity, at least up to a point. However, as the calcination temperature is increased beyond 900 °C, some metastable anatase crystals grow and transform into large rutile crystals. Although rutile has a lower band-gap

(3.0 eV) than anatase, well crystallized anatase has been identified as the most active TiO_2 phase under UV irradiation thanks to a higher reduction potential and a lower recombination rate of electron-hole pairs.[2b,3a] In addition, high calcination temperatures also lead to more significant grain growth leading to smaller surface areas. When the shell samples reported here were calcined to 900 °C or 950 °C, the surface area was seen to decrease markedly, to 19 and 14 m^2/g respectively (Figure 7b). Accordingly, although the H-TiO_2-900 sample displayed good anatase crystallinity, its catalytic activity was lower than that of H-TiO_2-800.

3. Conclusions

We have developed a simple yet effective method for synthesizing hollow mesoporous TiO_2 nanoshells with well-controlled crystallinity and phase, and demonstrated an ability to optimize their structure for enhanced performance in photocatalysis. This synthetic method involves TiO_2 coating on a SiO_2 colloidal template to form SiO_2@TiO_2 core-shell composites through a sol-gel process, base etching to remove the SiO_2 core, acid treatment to remove sodium ions, and finally calcination to produce hollow TiO_2 shells with tunable crystallinity and controllable phase. Acid treatment is the key step which addresses the prior challenges in maintaining the shell structure while controlling the phase and crystallinity. By converting undesired sodium titanates into protonated titanates, we have been able to not only prevent the formation of impurity phases, but also maintain the mesoscale porosity and the structural integrity of the shells, and also to control the development of the TiO_2 crystalline domains. This approach affords the fine tuning of the structure of the hollow TiO_2 shells toward an efficient photocatalyst that outperforms commercial P25-TiO_2 samples in the photocatalytic decomposition of organic dye molecules.

4. Experimental Section

Synthesis: Colloidal silica templates were prepared through a modified Stöber method.[19] Tetraethyl orthosilicate (TEOS, 99%, 0.86 mL) was mixed with the de-ionized water (4.3 mL), ethanol (23 mL) and an aqueous solution of ammonia (28%, 0.46 mL). After stirring for 4 h, the silica particles were separated by centrifugation, washed with ethanol, and then re-dispersed in 5 mL of ethanol. The above silica solution was well dispersed in a mixture of hydroxypropyl cellulose (HPC, 0.2 g), ethanol (95 mL), and de-ionized water (0.48 mL). After stirring for 30 min, tetrabutyl titanate (TBOT, 4 mL) in 18 mL of ethanol was injected into the mixture using a syringe pump at a rate of 0.5 mL/min. After injection, the temperature was increased to 85 °C at 900 rpm stirring under refluxing conditions for 100 min. The precipitate was isolated by centrifugation, washed with ethanol, and re-dispersed in 20 mL of water to give SiO_2@TiO_2 core-shell composites. To obtain hollow shells by removal of the SiO_2 core, an aqueous NaOH solution (4 mL, 2.5 M) was added to the solution, which was then stirred for 6 h. After etching, the TiO_2 shells were isolated by centrifugation, washed with de-ionized water and ethanol, dried under vacuum, dispersed in de-ionized water (150 mg/10 mL), mixed with an aqueous HCl solution, and stirred for 30 min. The resulting precipitates were isolated by centrifugation, washed with de-ionized water and ethanol, dried under vacuum, and calcined at the desired temperature for 2 h in air to obtain crystalline hollow TiO_2 shells.

Characterization: The sample morphology was characterized using TEM (Tecnai12). Crystal phases were determined by XRD analysis using a Bruker D8 advance diffractometer with Cu-Kα radiation (λ = 1.5406 Å). XPS spectra were obtained using a Kratos AXIS ULTRA^{DLD} XPS system equipped with an Al Kα monochromated X-ray source and a 165-nm electron energy hemispherical analyzer. Nitrogen adsorption isotherms were obtained at 77 K using a nitrogen sorption instrument (Quantachrome NOVA 4200e). Zeta potential measurement of the particle dispersion in water was conducted on a Beckman Coulter Delsa Nano C particle analyzer.

Catalytic Activity Tests: The photocatalytic activity was evaluated by following the degradation of Rhodamine B (RhB) as a function of time. Before the photocatalytic test was initiated, the catalyst was first irradiated under UV light for 30 min to remove any residual organic contaminants. The catalyst (5 mg) was dispersed in an aqueous RhB solution (25 mL, 2×10^{-5} M) in a 50 mL reactor cell and the solution was stirred in dark condition for 30 min to ensure adsorption of the dye on the catalyst surface. A 300 W Hg lamp with a 365 nm filter was used as the source of excitation (Xujiang XPA-7). The concentration of RhB was measured using a UV-Vis spectrophotometer (HR2000CG-UV-NIR, Ocean Optics). The concentration of RhB in the reaction media was followed as a function of time by using the intensity of the 553 nm absorption peak in order to obtain the kinetic data reported in Figure 8.

Supporting Information

Supporting Information is available from the Wiley Online Library or from the author.

Acknowledgements

Financial support for this project was provided by the U.S. Department of Energy (DE-FG02-09ER16096). Yin also thanks the Research Corporation for Science Advancement for the Cottrell Scholar Award and DuPont for the Young Professor Grant. F.Z. acknowledges additional funding from the U.S. National Science Foundation. The XPS facility used for the XPS characterization was developed thanks to funds from NSF grant DMR-0958796.

Received: January 22, 2013
Revised: February 18, 2013

---

[1] a) Z. Lu, M. Ye, N. Li, W. Zhong, Y. Yin, *Angew. Chem. Int. Ed.* **2010**, *49*, 1862–1866; b) Z. Lu, L. He, Y. Yin, *Chem. Commun.* **2010**, *46*, 6174–6176; c) Z. Wang, X. W. Lou, *Adv. Mater.* **2012**, *24*, 4124–4129; d) J. S. Chen, D. Luan, C. M. Li, F. Y. C. Boey, S. Qiao, X. W. Lou, *Chem. Commun.* **2010**, *46*, 8252–8254; e) J. S. Chen, L. A. Archer, X. Wen Lou, *J. Mater. Chem.* **2011**, *21*, 9912–9924; f) H. Choi, W. T. Chen, P. V. Kamat, *ACS Nano* **2012**, *6*, 4418–4427; g) J. Zhang, J. H. Bang, C. Tang, P. V. Kamat, *ACS Nano* **2009**, *4*, 387–395; h) I. Lee, J. B. Joo, Y. Yin, F. Zaera, *Angew. Chem., Int. Ed.* **2011**, *50*, 10208–10211; i) H. J. Yun, H. Lee, J. B. Joo, N. D. Kim, J. Yi, *Electrochem. Commun.* **2010**, *12*, 769–772; j) H. J. Yun, H. Lee, J. B. Joo, N. D. Kim, M. Y. Kang, J. Yi, *Appl. Catal. B* **2010**, *94*, 241–247; k) H. J. Yun, H. Lee, J. B. Joo, W. Kim, J. Yi, *J. Phys. Chem. C* **2009**, *113*, 3050–3055; l) M. Dahl, S. Dang, J. Bong Joo, Q. Zhang, Y. Yin, *CrystEngComm* **2012**, *14*, 7680–7685.
[2] a) A. Fujishima, K. Honda, *Nature* **1972**, *238*, 37–38; b) M. A. Fox, M. T. Dulay, *Chem. Rev.* **1993**, *93*, 341–357; c) A. Fujishima, X. Zhang, D. A. Tryk, *Surf. Sci. Rep.* **2008**, *63*, 515–582.
[3] a) A. L. Linsebigler, G. Lu, J. T. Yates, *Chem. Rev.* **1995**, *95*, 735–758; b) Q. Zhang, J.-B. Joo, Z. Lu, M. Dahl, D. Oliveira, M. Ye, Y. Yin,

Nano Res. **2011**, *4*, 103–114; c) Q. Zhang, D. Q. Lima, I. Lee, F. Zaera, M. Chi, Y. Yin, *Angew. Chem. Int. Ed.* **2011**, *50*, 7088–7092; d) K. Maeda, K. Domen, *J. Phys. Chem. Lett.* **2010**, *1*, 2655–2661; e) Y. Ao, J. Xu, D. Fu, C. Yuan, *J. Hazard. Mater.* **2009**, *167*, 413–417.

[4] a) J. Lee, M. Christopher Orilall, S. C. Warren, M. Kamperman, F. J. DiSalvo, U. Wiesner, *Nat. Mater.* **2008**, *7*, 222–228; b) X. Chen, L. Liu, P. Y. Yu, S. S. Mao, *Science* **2011**, *331*, 746–750; c) T. Cao, Y. Li, C. Wang, C. Shao, Y. Liu, *Langmuir* **2011**, *27*, 2946–2952; d) A. F. Demirörs, A. van Blaaderen, A. Imhof, *Chem. Mater.* **2009**, *21*, 979–984.

[5] T. R. Gordon, M. Cargnello, T. Paik, F. Mangolini, R. T. Weber, P. Fornasiero, C. B. Murray, *J. Am. Chem. Soc.* **2012**, *134*, 6751–6761.

[6] a) B. Wu, C. Guo, N. Zheng, Z. Xie, G. D. Stucky, *J. Am. Chem. Soc.* **2008**, *130*, 17563–17567; b) T. J. Trentler, T. E. Denler, J. F. Bertone, A. Agrawal, V. L. Colvin, *J. Am. Chem. Soc.* **1999**, *121*, 1613–1614.

[7] a) H. Li, Z. Bian, J. Zhu, D. Zhang, G. Li, Y. Huo, H. Li, Y. Lu, *J. Am. Chem. Soc.* **2007**, *129*, 8406–8407; b) X. Liu, Y. Gao, C. Cao, H. Luo, W. Wang, *Langmuir* **2010**, *26*, 7671–7674; c) D. Chen, L. Cao, F. Huang, P. Imperia, Y.-B. Cheng, R. A. Caruso, *J. Am. Chem. Soc.* **2010**, *132*, 4438–4444.

[8] a) A. Imhof, *Langmuir* **2001**, *17*, 3579–3585; b) J. W. Lee, M. R. Othman, Y. Eom, T. G. Lee, W. S. Kim, J. Kim, *Microporous Mesoporous Mater.* **2008**, *116*, 561–568.

[9] a) J. B. Joo, Q. Zhang, M. Dahl, I. Lee, J. Goebl, F. Zaera, Y. Yin, *Energy Environ. Sci.* **2012**, *5*, 6321–6327; b) J. B. Joo, Q. Zhang, I. Lee, M. Dahl, F. Zaera, Y. Yin, *Adv. Funct. Mater.* **2012**, *22*, 166–174; c) J. B. Joo, P. Kim, W. Kim, J. Kim, N. D. Kim, J. Yi, *Curr. Appl. Phys.* **2008**, *8*, 814–817; d) T. H. Eun, S.-H. Kim, W.-J. Jeong, S.-J. Jeon, S.-H. Kim, S.-M. Yang, *Chem. Mater.* **2009**, *21*, 201–203; e) P. Wang, D. Chen, F.-Q. Tang, *Langmuir* **2006**, *22*, 4832–4835.

[10] a) Y. Hu, J. Ge, Y. Sun, T. Zhang, Y. Yin, *Nano Lett.* **2007**, *7*, 1832–1836; b) Z. Zhong, Y. Yin, B. Gates, Y. Xia, *Adv. Mater.* **2000**, *12*, 206–209; c) H. G. Yang, H. C. Zeng, *J. Phys. Chem. B* **2004**, *108*, 3492–3495.

[11] J. Li, H. C. Zeng, *J. Am. Chem. Soc.* **2007**, *129*, 15839–15847.

[12] M. Ye, Q. Zhang, Y. Hu, J. Ge, Z. Lu, L. He, Z. Chen, Y. Yin, *Chem. Eur. J.* **2010**, *16*, 6243–6250.

[13] L. L. Hench, J. K. West, *Chem. Rev.* **1990**, *90*, 33–72.

[14] a) D. Yang, Z. Zheng, H. Liu, H. Zhu, X. Ke, Y. Xu, D. Wu, Y. Sun, *J. Phys. Chem. C* **2008**, *112*, 16275–16280; b) N. Li, L. Zhang, Y. Chen, M. Fang, J. Zhang, H. Wang, *Adv. Funct. Mater.* **2012**, *22*, 835–841; c) H. Kochkar, A. Turki, L. Bergaoui, G. Berhault, A. Ghorbel, *J. Colloid Interface Sci.* **2009**, *331*, 27–31.

[15] a) V. Bem, M. C. Neves, M. R. Nunes, A. J. Silvestre, O. C. Monteiro, *J. Photochem. Photobiol., A* **2012**, *232*, 50–56; b) H.-K. Seo, G.-S. Kim, S. G. Ansari, Y.-S. Kim, H.-S. Shin, K.-H. Shim, E.-K. Suh, *Sol. Energy Mater. Sol. Cells* **2008**, *92*, 1533–1539.

[16] a) S. Zhang, L. M. Peng, Q. Chen, G. H. Du, G. Dawson, W. Z. Zhou, *Phys. Rev. Lett.* **2003**, *91*, 256103; b) Y. Mao, M. Kanungo, T. Hemraj-Benny, S. S. Wong, *J. Phys. Chem. B* **2005**, *110*, 702–710; c) S. Zhang, Q. Chen, L. M. Peng, *Phys. Rev. B: Condens. Matter Mater. Phys.* **2005**, *71*, 014104; d) P. Wen, H. Itoh, W. Tang, Q. Feng, *Microporous Mesoporous Mater.* **2008**, *116*, 147–156.

[17] D. H. Hanaor, C. Sorrell, *J. Mater. Sci.* **2011**, *46*, 855–874.

[18] J. Zhong, F. Chen, J. Zhang, *J. Phys. Chem. C* **2009**, *114*, 933–939.

[19] W. Stöber, A. Fink, E. Bohn, *J. Colloid Interface Sci.* **1968**, *26*, 62–69.